Advances in Translational Medicine
https://ojs.luminescience.cn/ATM

LUMINESCIENCE
https://luminescience.cn/

Original Research

Real-time delineation of basement membrane in human oral and esophageal mucosa with micro-optical coherence tomography

Si Chen[1], Xin Ge[2], Xinyu Liu[1], Nanshuo Wang[1], Qiaozhou Xiong[1], Xiaojun Yu[3], Jinhan Li[4,5], Qianshan Ding[1,6], Linbo Liu[1,*]

[1] School of Electrical and Electronic Engineering, Nanyang Technological University, Singapore
[2] School of Science, Shenzhen Campus of Sun Yat-sen University, Shenzhen, China
[3] School of Automation, Northwestern Polytechnical University, Xi'an, Shanxi Province, China
[4] Beijing Jiaotong University, Beijing, China
[5] China Railway Siyuan Survey and Design Group Company Ltd., Wuhan, Hubei Province, China
[6] Department of Gastroenterology, Renmin Hospital of Wuhan University, Wuhan, Hubei Province, China

* Corresponding: liulinbo@ntu.edu.sg

Abstract:
Basement membrane is a thin, extracellular matrix-like structure, separating the epithelium from the stroma and having a vital role in determining cancer progression. Identification of this diagnostically important structure with histology is invasive and labor-intensive. Micro-optical coherence tomography (μOCT) which has the capability to recognize subcellular-level microstructures underneath the surface offers the possibility to resolve basement membrane noninvasively in situ and *in vivo*. In this study, we conducted numerical analysis of the back-scattering intensity of basement membrane and experimental μOCT imaging of human labial mucosa *in vivo* and esophageal mucosa *ex vivo*, in an attempt to characterize the basement membrane underlying stratified squamous epithelial tissues. The results disclose that the layered structure of mucosa could be clearly delineated and the basement membrane presented as a steep, low-scattering linear structure in between the relatively high-scattering epithelium and stroma. Besides, according to the knowledges on its ultrastructure, we assume the low-scattering signal is collectively determined by basal lamina and reticular lamina since the former alone is extremely thin to be recognized by μOCT. This study clarifies the scattering features of basement membrane and the capability of real-time delineation of basement membrane which will help to determine the progression of epithelial cancers without the need of resection and histology.

Keywords: Optical coherence tomography, Basement membrane, Oral mucosa, Esophagus, Optical imaging

Introduction

Basement membrane is an amorphous and sheet-like structure underlying the epithelium or surrounding muscle, fat and nerve axons [1]. Generally, it is composed of basal lamina and reticular lamina with a thickness of 50-100 nm, providing mechanical support to adjacent cells and regulating cell behaviors. In mucosa, this structure divides the epithelium from underlying stroma and has a vital role in determining the progression of diseases, such as in the cases of epithelial cancer. At the early stage of neoplasia, the basement membrane is intact; at an advanced stage,

Received: Jul.18, 2022; Revised: Oct.9, 2022; Accepted: Oct.11, 2022; Published: Oct.14, 2022

DOI: https://doi.org/10.55976/atm.1202219936-44

the neoplastic epithelial cells might produce a collagenolytic enzyme which potentially permeates to the basement membrane, so that neoplastic cells have ready access to nutrition and growth factors in the stroma which results in the rapid invasion or metastasis. Therefore, the identification of basement membrane has been an important theme in clinical workflow for cancer staging. In clinical practice, histology with special stains such as periodic acid-schiff (PAS) stain or sliver stain are often adopted to highlight such an extracellular matrix (ECM)-like structure. However, histology requires excisional biopsy which is both labor-intensive and time-consuming and makes it impossible to identify this structure during on-going examination.

Commercially available tomographic imaging modalities including computed tomography, ultrasound imaging, and magnetic resonance imaging, they can offer the possibility to visualize subsurface structures in real time [2]. However, their spatial resolution is far from sufficient to identify the basement membrane. Optical reflectance imaging tools such as confocal microscopy (CM), optical coherence tomography (OCT) and microscopy (OCM), and full field OCT (FF-OCT) afford spatial resolution at a scale comparable to histology offering the possibilities to identify this structure in real time [2-5]. In particular, OCT provides depth-resolved, cross-sectional images affording a spatial resolution of approximately 1-15 μm and a penetration depth of about 2-3 mm, and has been a well-established tool for visualizing microstructural details underneath the surface [2,6,7]. Functioning as a promising "optical biopsy" candidate, it has been used to image the basement membranes underlying stratified squamous epithelia in organs such as oral cavity [8-10], oropharynx [9], larynx [11,12], and cervix [13,14].

However, all of those previous OCT studies defined basement membrane based on the signal or intensity variations at the transitional region between the epithelium and the stroma by using system with the axial resolution limited to 6-10 μm [8-14]. In principle, this approach is not informative since the ECM-like basement membrane is too thin to be resolved at this resolution [8-14]. Consequently, the scattering characteristics of basement membrane is not clear, either a high-scattering region [8,13,15,16] or a low-scattering [17,18] region relative to adjacent stroma having been interpreted as the basement membrane.

μOCT, a cellular-resolution OCT system, provides the real-time cross-sectional images of tissues with a spatial resolution of 1-2 μm which is around one order of magnitude higher than the standard OCT technology. Previous studies have demonstrated its capability to recognize subcellular structures underneath the surface in tissues like atherosclerotic coronary artery wall [7], oral mucosa and esophageal mucosa [19]. To uncover the scattering characteristics of basement membrane underlying the epithelium, in this study we simulated the scattering feature of basement membrane numerically and validated the simulation results in human oral and esophageal mucosa experimentally using μOCT.

Methods

Simulation of back-scattering intensity of basement membrane

The image formation process of μOCT system was simulated using Matlab (MathWorks, Massachusetts, USA) on the basis of the scalar diffraction theory and the optical parameters of the sample arm optics. As the basement membrane structure appears to have an axial gap in the OCT image, we focused on the axial PSF in this study. The full-width at half-maximum of PSF profile is 1.8 μm in air, which corresponds to the axial resolution of the OCT imaging system. As shown in Figure 2(b), we generated a one-dimensional signal that represents the imaged basement membrane along the depth direction. We assume that the refractive index (RI) distribution of mucosal layers surrounding the basement membrane is random, which is normalized between 0 and 1. The unit displacement to oversample the 200 nm gap representing the basement membrane is 20 nm, which is one-tenth of the gap width. The output of the imaging system is calculated by a convolution of the simulated ideal PSF with the above-mentioned refractive index distribution along the depth direction. 10 RI signal cases were convolved with the PSF function to generate output signals, as shown in Figure 2(c). As a result, we averaged all the output signals to simulate the OCT depth profile.

μOCT imaging system

A previously developed μOCT system was used in this study [19,20]. Briefly, the light went to reference arm and sample arm respectively after being divided by a beam splitter (PAFA-X-4-B, Thorlabs, New York). The back-reflected or back-scattered light from the reference arm and the sample arm were combined by the same beam splitter and directed by a single-mode fiber (630-HP, Nufern, USA) to a spectrometer which thereafter transferred the interference spectra to the computer through an image acquisition board (KBN-PCE-CL2-F, Bitflow, USA). We used a supercontinuum light source (SC-5, Yangtze Soton Laser, Wuhan, China) centered at 800 nm with full width at half maximum of ~180 nm to achieve a measured axial resolution of ~1.8 μm in air which corresponds to 1.3 μm in tissue with refractive error of 1.38 (Figure 1a). The axial resolution over depth is consistently higher than 2 μm in air as shown in our previous study [21]. The total ranging depth is ~1.4 mm and the sensitivity roll-off is ~6 dB/mm. The sample arm was constructed to be a compact handheld probe for image acquisition *in vivo*. The probe was

composed of a collimation lens (achromat, f = 15 mm, AC050-015-B-ML, Thorlabs, USA) and an objective lens (M Plan Apo NIR 20X, Mitutoyo, Japan) to achieve a transverse resolution of 1.8 µm. The lateral resolution was evaluated by a resolution target where the resolution chart bar periods of better than 4.4 µm can be clearly resolved (Figure 1b).

A glass window (fused silica, Diameter = 2 mm) was assembled about 100 µm before the focal plane of the objective lens to maintain the working distance between the lens and the tissues for *in vivo* studies. The system acquired three-dimensional dataset over a size of 1024 × 1024 × 2048 (x × y × z) and the axial line rate was 20,000 Hz (20 frames/s) and 60,000 Hz (60 frames/s) for *ex vivo* and *in vivo* imagings, respectively. The axial line rate was higher for *in vivo* studies to enable real-time image acquisition and to avoid motion artifacts.

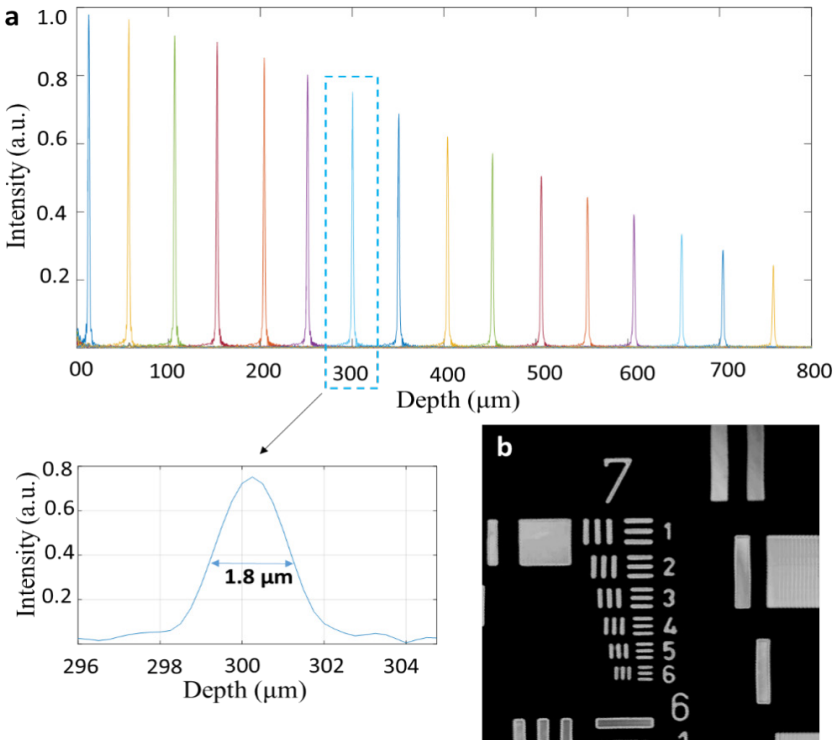

Figure 1. Characterization of spatial resolutions of µOCT imaging system
(a) Axial point spread functions were measured over the optical path delay of 0-800 µm. The axial resolution was measured at the full width at half maximum. (b) An en face image of USAF resolution chart. The radius of the focal spot is 1.8 µm and the resolution chart bar periods of better than 4.4 µm can be clearly resolved.

µOCT imaging of basement membrane in human oral and esophageal mucosa

We acquired µOCT images of nonkeratinized oral mucosa (labial mucosa) from 2 human subjects in vivo. The imaging field of view was 872 × 436 µm (x × y) *in vivo*. The glass window of the handheld probe was sterilized with 75% ethanol solution prior to µOCT imaging. After sterilization, the glass window of the flexible probe was coated with disposable food packing thin film and was gently positioned on the surface of the labial mucosa for image acquisition. Written consents were obtained from these two subjects before the experiment and the study was approved by the Institutional Review Board (IRB) of Nanyang Technological University (NTU) (IRB-2016-10-015).

We also conducted µOCT imaging of the clean margin of esophageal specimens from 3 patients *ex vivo* (1 diagnosed with superfical esophageal carcinoma and 2 with high-grade intraepithelial neoplasia). Immediately after the resection of suspicious lesions endoscopically, the specimens were sent to the imaging site and OCT images were acquired at 3-4 locations of the clean margin (Lugol's positive) for each specimen. *Ex vivo* µOCT images were obtained from the clear margins of the specimens with a field of view of 872 × 872 µm (x × y). Following µOCT imaging, the specimens were fixed with 10% neutral buffered formalin overnight and submitted to tissue processing. Sections from the clean margin of the specimens with 5-µm-thick were stained with periodic acid-Schiff (PAS) to highlight basement membrane. Written consents were obtained from the patients before the endoscopic operation. The use of human specimens was approved by the IRB at Renmin Hospital of Wuhan University (2017K-C053).

Result

Simulation results on reflectance contrast of the basement membrane

Based on the assumption that the refractive index distribution of the basement membrane is homogeneous and that of the surrounding tissues are heterogeneous, our simulation numerical analysis showed that basement membrane presented a low scattering intensity relative to adjacent high-scattering tissues (Figure 2d). The axial profile of the basement membrane (Figure 2b) is apparently broadened by the convolution with the axial PSF of µOCT. Although the axial resolution of µOCT is not enough to resolve the upper than lower borders of the basement membrane, its characteristic scattering contrast with regard to the surrounding epithelial and connective tissues makes it possible to detect the basement membrane in µOCT images.

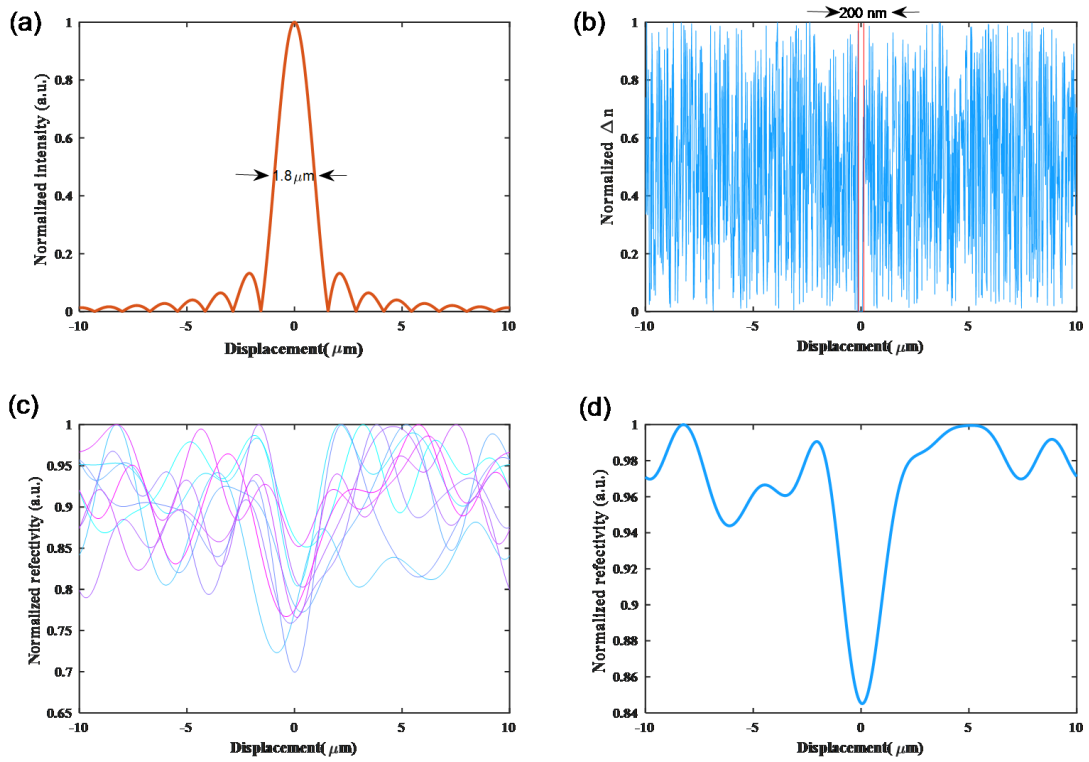

Figure 2. Theoretical analysis of back-scattered intensity of basement membrane
(a) Intensity point spread function of the light incident on the sample. The full-width at half-maximum is 1.8 µm in air corresponding to the axial resolution of the µOCT system used in this study. (b) A representative refractive index difference distribution between basement membrane and its overlying and underlying structures. The zero displacement represents basement membrane with a thickness of ~200 nm and a homogenous refractive index distribution (Δn = 0). The refractive indexes of the tissues surrounding basement membrane were randomly generated and a total of 10 cases were generated in this study. (c) The simulation results of intensity distribution with each line representing one case of refractive index difference. (d) Averaged intensity of the 10 cases presented in (c) contributing to basement membrane with a steep low-scattering intensity.

Basement membrane in human labial mucosa

Figure 3 shows a representative µOCT image from a human subject *in vivo*. The mucosal layers including the epithelium, basement membrane and lamina propria could be readily differentiated in the cross-sectional µOCT images. The basement membrane demonstrated as a uniform, continuous low-scattering thin line which was distinct from the epithelium and the underlying stroma by the steep contrast change (Figure 3b, yellow arrows). Subcellular structures such as nuclei of keratinocytes could also be differentiated in µOCT images (Figure 3b, white arrows). The thickness of epithelium was measured to be 140.66 ± 0.63 µm. The image of the basement membrane is 2.27 ± 0.08 µm (mean ± standard error; n=50) in depth, which is theoretically a result of convolution between the axial point spread function and the basement membrane depth profile and does not directly reflect the thickness of the basement membrane.

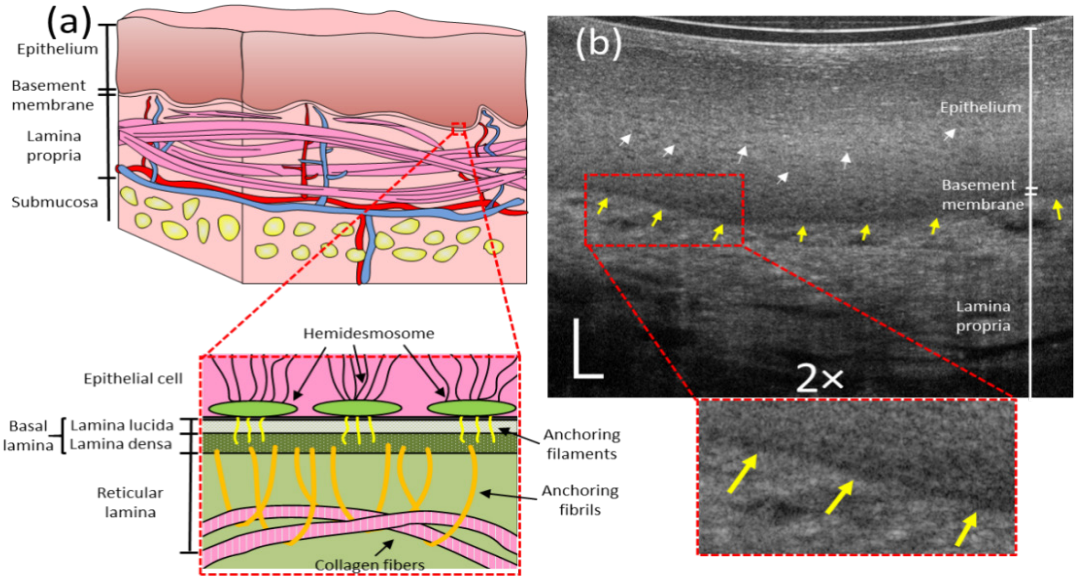

Figure 3. µOCT imaging of labial mucosa from a human subject (female, 30 years old) in *vivo*.
(a) Schematics of human labial mucosa and the zoomed-view shows the ultrastructure of basement membrane region. (b) A representative cross-sectional µOCT image: the yellow arrows indicate the basement membrane and the white arrows represent nuclei. Scale bars, 50µm.

We also evaluated the visibility of basement membrane in human labial mucosa when the axial resolution of µOCT was algorithmically degraded to 5 µm (Figure 4). In the images acquired by µOCT with axial resolution of 1.8 µm in air *in vivo*, the mucosal layers were clearly differentiated with the basement membrane presenting as a thin low-scattering line (Figure 4a) and well demarcated by the steep change in the scattering intensity (Figure 4b, red arrows). In contrast to the tomograms acquired by µOCT (Figure 4a), when the axial resolution was algorithmically degraded to 5 µm in air, the basement membranes became much less uniform and the contrast against the epithelium and the stroma was much less discernable (Figure 4c); the shape of the intensity valley of the basement membrane (Figure 4d, red arrows) was difficult to be differentiated from that of a neighboring structure on the axial profile of the optical signals (Figure 4d, green arrows).

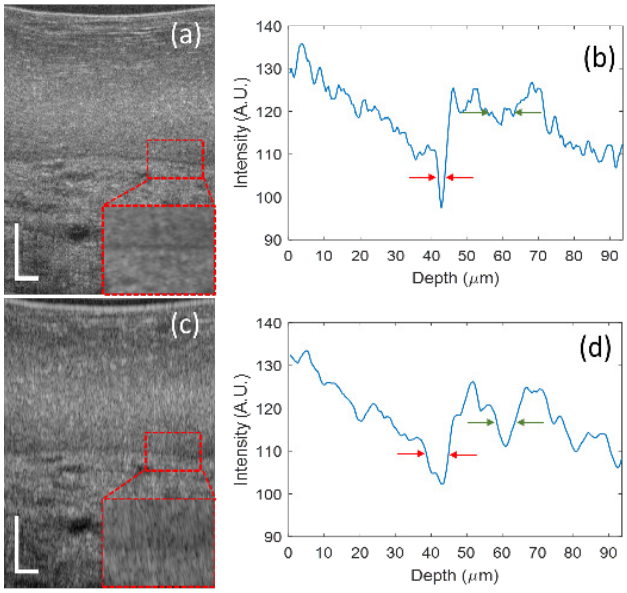

Figure 4. Comparison of μOCT images from human labial mucosa (male, 38 years old) before and after the axial resolution was algorithmically degraded

(a) A representative μOCT tomograms : basement membrane could be clearly recognized and areas in red dashed box were zoomed in by 2X presenting the clearly-defined, low-scattering basement membrane; (b) corresponding axial profile of optical signals: the red arrows indicate the basement membrane and the green arrows show regions with irregularly decreased optical intensity. (c) OCT tomograms with axial resolution degraded to 5 μm in air and red dashed box were zoomed in by 2X demonstrating that basement membrane was difficult to be identified; (d) corresponding axial profile of optical intensity: the basement membrane area (red arrows) and a neighbouring structure (green arrows) present similar low-intensity profile making it difficult to differentiate these two structures. Scale bars, 50 μm.

Basement membrane in the human esophagus

Similar to those observed in human labial mucosa, the basement membrane of the esophageal mucosa was low scattering (Figure 5a). It appeared as a continuous, uniform thin line with good scattering contrast against overlying epithelium and underlying connective tissues (Figure 5a). Subcellular structures including cell nuclei could also be resolved (Figure 5a, white arrows). Figure 5b is a representative histological image with PAS staining from the clear margin of the esophageal specimen and the basement membrane and the cytoplasm of those well-differentiated keratinocytes demonstrated PAS positive.

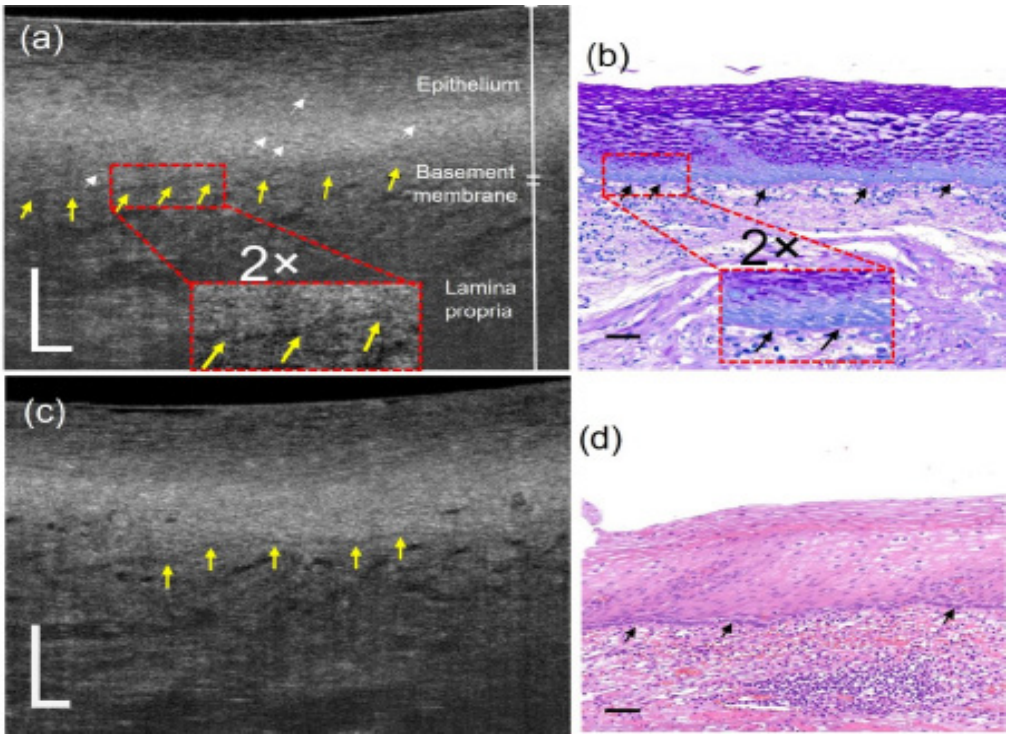

Figure 5. μOCT imaging of the clean margin of esophageal specimens from patients *ex vivo*

(a,b) Representative μOCT cross-sectional image of the clean margin of a 72-year-old, female patient with superfical esophageal carcinoma (a) and the corresponding histology with Periodic acid-Schiff (PAS) staining (b): yellow arrows in (a) and black arrows in (b) indicate PAS-positive basement membrane; white arrows in (a) suggest cell nuclei. (c-d) Respresentative μOCT cross-sectional image from the clean margin of a 59-year-old, female patient with high-grade intraepithelial neoplasia (c) and corresponding histology with HE staining (d): yellow arrows in (c) and black arrows in (d) indicate basement membrane. Scale bars, 50 μm.

Discussion

The current study for the first time demonstrates the capability of μOCT to reliably detect the basement membrane in the human mucosa of internal organs *in vivo*. Similar to routine light microscopy, the basement membrane is consisted of basal lamina and reticular lamina with a thickness of 50-100 nm and 0.2-4 μm, respectively that is beyond the reach of optical resolution [1,22] and thus cannot be resolved by μOCT. According to the knowledge from previous transmission electron microscopy, the basal lamina could be further divided into an electron-lucent layer (lamina lucida) and an electron-dense layer (lamina densa), in association with a considerably thicker reticular lamina which is a layer of loose connective tissue and presumably low scattering in OCT images. Since the basal lamina is extremely thin, it is likely that the basal lamina and particularly the reticular

lamina collectively contributes to the low-scattering linear structure in-between the relatively high-scattering epithelium and stroma in μOCT images, which has not been clearly interpreted in previous studies.

In our study, the basement membrane is not clearly detected at all locations. We suspect that it is because of the incident angle relative to the basement membrane: it is imaged with good visibility if the incident angle is close to 90-degree. However, since the orientation of the basement membrane may vary with papillary structure of the mucosa, the scattering contrast may have been altered. This issue may be mitigated by flattening the mucosa during imaging.

It is not informative to simply attribute the low scattering variations at the transitional region between the epithelium and the stroma to the basement membrane without actually seeing it, because one would not know if the basement membrane is intact or not. In contrast, this study clearly delineated this fine structure from the adjacent tissues by the use of μOCT. The basement membrane as in μOCT images of human oral and esophageal mucosa is a uniform, continuous thin low-scattering line, well demarcated by the steep change in the scattering intensity. The capability of visualizing basement membrane directly at such a clarity would provide confidence in determining the integrity of this structure. Analogues to the studies in understanding the scattering properties of the dermoepidermal junction in skin [15,18,23-25], previous OCT studies which proposed the basement membranes of mucosa in the oral [8] and cervical mucosa [13] were high-scattering (or bright) might have misinterpreted the adjacent high-scattering stroma as the basement membrane. This misinterpretation is probably due to the insufficient resolution of their imaging systems whose axial resolution is 10 and 6 μm respectively [8,13].

The axial resolution of μOCT is still not enough to directly measure the thickness of the basement membrane. It is extremely challenging, if possible at all, to resolve the upper and lower boundary of the basement membrane, simply because the axial resolution limit of OCT is ~0.5 μm for the visible light. However, it is still possible to apply super-resolution techniques, such as deconvolution, for quantitative evaluation. Of course, measures that guarantee sufficient signal to noise ratio and speckle suppression are needed to avoid image artifacts. We hope this study will facilitate further discussions on the potential applications of quantitative information that may be available with μOCT.

In this study, we demonstrated the optical scattering characteristics of basement membrane in normal human oral and esophageal mucosa. The limitation of this study is that the thicknesses of basement membranes are manually measured in limited subjects. Studies involving a large number of volunteers are necessary to establish the average thickness of this structure in population. Besides, with the capability of identifying basement membrane, future studies are required to evaluate the diagnostic performance of μOCT in differentiating intraepithelial neoplasia and cancer infiltration. In addition, although we are able to resolve the structure in human labial mucosa using a handheld probe *in vivo*, there is another limitation that we are currently impossible to identify this structure in internal organs such as larynx, esophagus, or cervix *in vivo* due to the lack of a flexible endoscopic probe. However, with the rapid development of μOCT transendoscopic probes [26,27], the real-time recognition of the basement membrane will have unprecedented significance for the diagnosis of the progression of cancers without the need of resection and subsequent histopathology.

Disclosure

The authors declare no conflict of interest.

Authors' contributions

S.C. X.G. and L.L. conceived and designed the study. X.G. condunumerical simulation. S.C., X.L., N.W.,Q.X., X.Y., J.L.,Q.D. participated in experimental verifications and data analysis. S.C. X.G. and L.L. prepared manuscript.

Acknowledgements

This research is supported by the Singapore Ministry of Health's National Medical Research Council under its Cooperative Basic Research Grant(NMRC/CBRG/0036/2013) and Open Fund Individual Research Grant(MOH-000384), National Research Foundation Singapore under its Competitive Research Program(NRF-CRP13-2014-05) and the Ministry of Education Singapore under its Academic Research Funding Tier 2(MOE-T2EP30120-0001).

References

[1] Kalluri R. Basement membranes: structure, assembly and role in tumour angiogenesis. *Nature Reviews Cancer.* 2003;3(6): 422-433. doi: https://doi.org:10.1038/nrc1094

[2] Fujimoto J.G. Optical coherence tomography for ultrahigh resolution in vivo imaging. *Nature Biotechnology.* 2003;21(11): 1361-1367. doi: https://doi.org:10.1038/nbt892

[3] Tsai C.C., Chang C.K., Hsu K.Y., et al. Full-depth epidermis tomography using a Mirau-based full-field optical coherence tomography. *Biomedical Optics Express*. 2015;5(9): 3001-3010 . doi: https://doi.org:

10.1364/boe.5.003001
[4] Carlson K., Pavlova I., Collier T., et al. Confocal microscopy: imaging cervical precancerous lesions. *Gynecologic Oncology.* 2005;99(30): S84-88. doi: https://doi.org:10.1016/j.ygyno.2005.07.049
[5] Kang D., Suter M.J., Boudoux C., et al. Comprehensive imaging of gastroesophageal biopsy samples by spectrally encoded confocal microscopy. *Gastrointest Endoscopy.* 2010;71(1): 35-43. doi: https://doi.org:10.1016/j.gie.2009.08.026
[6] Drexler W., Morgner U., Ghanta R.K., et al. Ultrahigh-resolution ophthalmic optical coherence tomography. *Nature Medicine.* 2001;7(4): 502-507. doi: https://doi.org:10.1038/86589
[7] Liu L., Gardecki J.A., Nadkarni S.K., et al. Imaging the subcellular structure of human coronary atherosclerosis using micro-optical coherence tomography. *Nature Medicine.* 2011;17(8): 1010-1014. doi: https://doi.org:10.1038/nm.2409
[8] Wilder-Smith P.B., Krasieva T.B., Jung W.G., et al. Noninvasive imaging of oral premalignancy and malignancy. *Journal of Biomedical Optics*. 2005;10(5): 051601. doi: https://doi.org:10.1117/1.2098930
[9] Ridgway J.M., Armstrong W.B., Guo S., et al. In vivo optical coherence tomography of the human oral cavity and oropharynx. *Archives of Otolaryngology–Head & Neck Surgery*. 2006;132(10): 1074-1081. doi: https://doi.org:10.1001/archotol.132.10.1074
[10] Jerjes W., Upile T., Conn B., et al. In vitro examination of suspicious oral lesions using optical coherence tomography. *The British Journal of Oral & Maxillofacial Surgery.* 2010;48(1): 18-25. doi: https://doi.org:10.1016/j.bjoms.2009.04.019
[11] Wong B.J., Jackson R.P., Guo S., et al. In vivo optical coherence tomography of the human larynx: normative and benign pathology in 82 patients. *The Laryngoscope.* 2005;115(11): 1904-1911. doi: https://doi.org:10.1097/01.mlg.0000181465.17744.be
[12] Armstrong W.B., Ridgway J.M., Vokes D.E., et al. Optical coherence tomography of laryngeal cancer. *The Laryngoscope.* 2006;116(7): 1107-1113. doi: https://doi.org:10.1097/01.mlg.0000217539.27432.5a
[13] Pitris C., Goodman A., Boppart S.A., et al. High-resolution imaging of gynecologic neoplasms using optical coherence tomography. *Obstetrics & Gynecology.* 1999;93(1): 135-139. doi: https://doi.org/10.1016/S0029-7844(98)00375-5
[14] Escobar P.F., Belinson J.L., White A., et al. Diagnostic efficacy of optical coherence tomography in the management of preinvasive and invasive cancer of uterine cervix and vulva. *International Journal of Gynecological Cancer.* 2004;14(3): 470-474. doi: https://doi.org:10.1111/j.1048-891x.2004.14307.x
[15] Welzel J., Lankenau E., Birngruber, R., et al. Optical coherence tomography of the human skin. *Journal of the American Academy of Dermatology.* 1997;37(6): 958-963. doi: https://doi.org/10.1016/S0190-9622(97)70072-0
[16] Hariri L.P., Mino-Kenudson M., Mark E.J., et al. In vivo optical coherence tomography: the role of the pathologist. *Archives of Pathology & Laboratory Medicine.* 2012;136(12): 1492-1501. doi: https://doi.org:10.5858/arpa.2012-0252-SA
[17] Zeng X., Zhang X., Li C., et al. Ultrahigh-resolution optical coherence microscopy accurately classifies precancerous and cancerous human cervix free of labeling. *Theranostics.* 2018;8(11): 3099-3110. doi: https://doi.org:10.7150/thno.24599
[18] Israelsen N.M., Maria M., Mogensen M., et al. The value of ultrahigh resolution OCT in dermatology - delineating the dermo-epidermal junction, capillaries in the dermal papillae and vellus hairs. *Biomedical Optics Express.* 2018;9(5): 2240-2265. doi: https://doi.org:10.1364/BOE.9.002240
[19] Chen S., Ge X., Liu X., et al. Understanding optical reflectance contrast for real-time characterization of epithelial precursor lesions. *Bioengineering & Translational Medicine.* 2019;4(3): e10137. doi: https://doi.org:10.1002/btm2.10137
[20] Chen S., Liu X., Wang N., et al. Contrast of nuclei in stratified squamous epithelium in optical coherence tomography images at 800 nm. *Journal of Biophotonics.* 2019;12(9): e201900073. doi: https://doi.org:10.1002/jbio.201900073
[21] Yu X., Luo Y., Liu X., et al. Toward High-Speed Imaging of Cellular Structures in Rat Colon Using Micro-optical Coherence Tomography. *IEEE Photonics Journal.* 2016;8(4): 1-8. doi: https://doi.org:10.1109/JPHOT.2016.2589659
[22] Saglani S., Molyneux C., Gong H., et al. Ultrastructure of the reticular basement membrane in asthmatic adults, children and infants. *European Respiratory Journal.* 2006;28(3): 505-512. doi: https://doi.org:10.1183/09031936.06.00056405
[23] Weissman J., Hancewicz T. Kaplan P. Optical coherence tomography of skin for measurement of epidermal thickness by shapelet-based image analysis. *Optics Express.* 2004;12(23): 5760-5769. doi: https://doi.org/10.1364/OPEX.12.005760
[24] Boone M., Jemec G.B. Del Marmol V. High-definition optical coherence tomography enables visualization of individual cells in healthy skin: comparison to reflectance confocal microscopy. *Experimental Dermatology.* 2012;21(10): 740-744. doi: https://doi.org:10.1111/j.1600-0625.2012.01569.x
[25] Neerken S., Lucassen G.W., Bisschop M.A., et al. Characterization of age-related effects in human skin: A comparative study that applies confocal laser scanning microscopy and optical coherence tomography. *Journal of Biomedical Optics.* 2004;9(2): 274-281. doi: https://doi.org:10.1117/1.1645795
[26] Yin B., Chu K.K., Liang C.P., et al. μOCT imaging using depth of focus extension by self-imaging wavefront division in a common-path fiber optic probe. *Optics Express.* 2016;24(5): 5555-5564. doi:

https://doi.org:10.1364/OE.24.005555
[27] Luo Y., Cui D., Yu X., et al. Endomicroscopic optical coherence tomography for cellular resolution imaging of gastrointestinal tracts. *Journal of Biophotonics.* 2018;11(4): e201700141. doi: https://doi.org:10.1002/jbio.201700141